Spatiotemporal dynamics of triglyceride storage in unilocular adipocytes

Michael Chu[a], Harini Sampath[b], David Y. Cahana[c], Christoph A. Kahl[d], Romel Somwar[e], Anda Cornea[f], Charles T. Roberts, Jr.[a,c], and Oleg Varlamov[c]

[a]Division of Endocrinology, Diabetes, and Clinical Nutrition, Department of Medicine, and [b]Oregon Institute of Occupational Health Sciences, Oregon Health and Science University, Portland, OR 97239; [c]Divisions of Diabetes, Obesity, and Metabolism and Developmental and Reproductive Science, [d]Division of Pathobiology and Immunology, and [f]Division of Neuroscience, Oregon National Primate Research Center, Beaverton, OR 97006; [e]Department of Pathology, Memorial Sloan-Kettering Cancer Center, New York, NY 10065

ABSTRACT **The spatiotemporal dynamics of triglyceride (TG) storage in unilocular adipocytes are not well understood. Here we applied ex vivo technology to study trafficking and metabolism of fluorescent fatty acids in adipose tissue explants. Live imaging revealed multiple cytoplasmic nodules surrounding the large central lipid droplet (cLD) of unilocular adipocytes. Each cytoplasmic nodule harbors a series of closely associated cellular organelles, including micro–lipid droplets (mLDs), mitochondria, and the endoplasmic reticulum. Exogenously added free fatty acids are rapidly adsorbed by mLDs and concurrently get esterified to TG. This process is greatly accelerated by insulin. mLDs transfer their content to the cLD, serving as intermediates that mediate packaging of newly synthesized TG in the large interior of a unilocular adipocyte. This study reveals novel cell biological features that may contribute to the mechanism of adipocyte hypertrophy.**

Monitoring Editor
Jean E. Gruenberg
University of Geneva

Received: Jun 12, 2014
Revised: Sep 29, 2014
Accepted: Sep 30, 2014

INTRODUCTION

White adipose tissue (WAT) has a greater capacity to store lipids, primarily in the form of triglycerides (TGs) and sterol esters, than any other mammalian tissue. The expandable nature of WAT allows adipocytes to efficiently store and release free fatty acids (FFAs) in order to match energy supply with demand. WAT mediates the insulin-stimulated postprandial adsorption of FFA and glucose, the precursors for synthesis of TGs, which are subsequently stored in specialized organelles known as lipid droplets (LDs; reviewed in Brasaemle and Wolins, 2012; Khor *et al.*, 2013; Thiam *et al.*, 2013b). A single central LD (cLD) occupies the main volume of the unilocular adipocyte characteristic of mature WAT.

The intraleaflet space of the endoplasmic reticulum (ER) membrane bilayer is believed to be the primary site of TG synthesis and the source of nascent LDs that bud off the cytoplasmic face of the ER membrane bilayer (Thiam *et al.*, 2013b). LDs are surrounded by a phospholipid monolayer whose lipid composition differs from that of the ER bilayer (Tauchi-Sato *et al.*, 2002), suggesting that lipid sorting takes place at the interface of the ER and the LD. The packaging of TG into LDs is coordinated, in a spatiotemporal manner, by ensembles of proteins, which include, but are not limited to, the PAT family members perilipin, adipophilin (ADRP), TIP47, S3-12, and OXPAT/MLDP (reviewed in Brasaemle, 2007). LD-associated proteins represent a continuously growing family that orchestrates distinct lipid biosynthesis and lipolysis steps and/or are involved in LD budding from the ER membranes (Hommel *et al.*, 2010; Thiam *et al.*, 2013a; Wilfling *et al.*, 2014), interdroplet lipid exchange (Jambunathan *et al.*, 2011; Grahn *et al.*, 2013; Sun *et al.*, 2013), and homotypic fusion (Bostrom *et al.*, 2007).

Recently published studies using in vitro–differentiated 3T3-L1 adipocytes demonstrated that interdroplet lipid exchange at LD-LD contact sites, mediated by a cooperative action of Fsp27 (human CIDEC) and perilipin 1a, is responsible for LD growth and the development of a unilocular phenotype in adipocytes (Grahn *et al.*, 2013; Sun *et al.*, 2013). Although LD-LD fusion in adipocytes does occur,

This article was published online ahead of print in MBoC in Press (http://www.molbiolcell.org/cgi/doi/10.1091/mbc.E14-06-1085) on October 8, 2014.

The authors have no conflicting interests to disclose.

Address correspondence to: Oleg Varlamov (varlamov@ohsu.edu).

Abbreviations used: ACSL, acyl-CoA synthetase; cLD, central lipid droplet; ER, endoplasmic reticulum; FFA, free fatty acid; LD, lipid droplet; mLD, micro–lipid droplet; TG, triglycerides; TLC, thin-layer chromatography; WAT, white adipose tissue.

some investigators suggest that this phenomenon is a relatively infrequent event (Murphy *et al.*, 2010).

The average lifespan of a WAT adipocyte is significantly longer than that of a typical in vitro–differentiated adipocyte (years vs. weeks; Spalding *et al.*, 2008; Arner *et al.*, 2011). Furthermore, the former has a unique morphological architecture and a distinct geometric pattern of lipid packing: the cLD of a unilocular adipocyte represents a single sphere tightly fitted inside the cell, whereas LDs of multilocular adipocytes represent multiple spheres dispersed throughout the cytoplasm. The biogenesis of LDs in unilocular adipocytes is poorly understood due to the fragile nature of WAT. In this study, we applied live-cell imaging to describe the morphological and functional organization of TG synthesis in unilocular adipocytes.

RESULTS

To achieve better understanding of intracellular organization of unilocular adipocytes, we infected visceral WAT explants of nonhuman primates with an adenoviral vector encoding enhanced green fluorescent protein (eGFP) and examined living tissue by confocal microscopy. GFP labeled the cytoplasm and nuclei of adipocytes and stromo-vascular cells (Figure 1, A–F, large spherical and fibroblast-like cells, respectively). The cytoplasm of unilocular adipocytes appeared as a series of perforated nodules scattered around the cell surface (Figure 1, A–D). In addition, a thicker cytoplasmic layer surrounded adipocyte nuclei (Figure 1E). Perforated nodules were connected by a thin layer of GFP-positive cytoplasm (Figure 1, B and C). Each nodule harbored fluorescence-negative cavities that appeared as uniformly sized spheres. We hypothesized that these spheres represent preexisting micro-LDs (mLDs) filled with lipids. cLDs of each adipocyte were fluorescence-free (Figure 1B). A schematic diagram representing the spatial organization of a unilocular adipocyte is given in Figure 1G.

To elucidate the spatiotemporal dynamics of TG synthesis and packaging in unilocular adipocytes, we labeled WAT explants with the fluorescent FFA analogue BODIPY-C12. Previously, we and others demonstrated that BODIPY-FFA is transported into in vitro–differentiated adipocytes and WAT explants by an insulin-stimulated mechanism (Li *et al.*, 2005; Liao *et al.*, 2005; Wu *et al.*, 2006a,b; Varlamov *et al.*, 2010, 2012, 2013; Somwar *et al.*, 2011) and is esterified to BODIPY-TG in 3T3-L1 adipocytes (Sun *et al.*, 2013). Confocal microscopy analysis unveiled a striking, previously unobserved staining pattern that appeared as clusters of bright fluorescent mLDs scattered around the surface of the cLD (Figure 2, A and D, green). Each group of mLDs was surrounded by a distinct ER patch (Figure 2, red, and Supplemental Video S1). Three-dimensional reconstitution of confocal scans revealed "eggs-in-a-nest"-like structures, with mLDs occupying spherical cavities within each ER patch (Figure 2, B and E).

The mLDs were relatively uniform in size, with an average diameter of 0.7 µm (Figure 2C). The number of mLDs in the patch varied in WAT samples obtained from different animals, but the area occupied by LDs naturally correlated with the area of the surrounding ER (Figure 2, A and B, represents adipocytes with smaller ER patches, whereas Figure 2D represents an adipocyte with larger ER patches). When insulin-treated WAT explants were labeled with BODIPY-C12 and then subjected to indirect immunofluorescence analysis, antibodies to perilipin 1a decorated ring-like structures surrounding individual mLDs. In addition to mLD-associated rings, perilipin 1a also appeared as a diffuse coat outlining the surface of the cLD (Figure 2F).

We further examined the ultrastructural organization of mLDs in unilocular adipocytes using electron microscopy. Electron-lucent mLDs ranging up to 1 µm in diameter were frequently observed in adipocyte cytoplasm in the vicinity of or attached to the cLD (Figure 3A). mLDs were surrounded by or associated with mitochondria (Figure 3, A–C). Tubular membranes of the smooth ER decorated with budding vesicles were frequently observed in the areas containing mLDs and mitochondria (Figure 3, B–D, arrowheads). Furthermore, some mLDs were decorated by electron-lucent vesicular material, which may represent the ER or precursors of mLDs (Figure 3E). Of interest, rough ER membranes were not typically associated with mLDs (Figure 3F).

A close association of mLDs with the cLD and the ER suggests that mLDs may represent intermediary compartments mediating the packaging of newly synthesized TG into the cLD. To verify this hypothesis, we followed the time course of intracellular BODIPY-C12 transport by confocal microscopy. Control (basal) or insulin-treated WAT explants were pulsed with BODIPY-C12 for 15 min and then chased in label-free medium for different time periods. Insulin significantly stimulated the uptake of BODIPY-C12 into adipocytes (Figure 4, A and B). Immediately after an insulin pulse, fluorescence appeared in mLDs scattered around the cLD (Figure 4A, Ins 0h). After an insulin chase, mLD-associated fluorescence gradually decreased, whereas cLD-associated fluorescence concomitantly increased (Figure 4, A and C). Live-cell imaging of BODIPY-C12–labeled WAT explants verified that the disappearance of fluorescence from mLDs is concurrent with the appearance of fluorescence in cLDs (Figure 4D and Supplemental Video S2). Imaging BODIPY-C12–labeled WAT explants at higher spatiotemporal resolution revealed that individual mLDs discharge their fluorescent content with a half-time on the order of 50 s (Figure 4, E, circle, F, solid lines, and G, and Supplemental Video S3). Many mLDs remained static over a 10-min imaging interval (Figure 4, E, square, and F, dotted lines), suggesting that the observed disappearance of mLDs has a probabilistic nature. BODIPY-labeled palmitic acid (BODIPY-C16) and BODIPY-C12 showed similar kinetics of transport in unilocular adipocytes (unpublished data). Collectively, these results confirm a unidirectional transport of BODIPY-labeled lipids between mLDs and cLDs.

To verify that BODIPY-C12 is readily metabolized into BODIPY-TG, we pretreated WAT explants with basal or insulin-containing media, pulsed them for 15 min with BODIPY-C12, chased them in label-free media, and analyzed FFA metabolites by thin-layer chromatography (TLC). Under basal "no-chase" conditions, BODIPY-C12 migrated primarily as FFA, with only a minor fraction of total fluorescence incorporated into BODIPY-TG (Figure 5A, lane 1). After a chase in basal medium, the BODIPY-TG/BODIPY-C12 ratio increased, consistent with the slow basal rate of TG synthesis. In addition to apparent BODIPY-TG synthesis, there was a time-dependent accumulation of additional BODIPY-labeled species (Figure 5A, asterisk and bracket). Insulin treatment of WAT explants increased the BODIPY-TG/BODIPY-C12 ratio and stimulated the formation of additional BODIPY-labeled species in comparison with basal conditions (Figure 5A, compare lanes 2 and 1). After an insulin chase, BODIPY-C12 was progressively converted into TG (Figure 5A, compare lanes 2, 4, and 6).

Pretreatment of WAT explants with triacsin C, an inhibitor of the long-chain Acyl-CoA synthetase (ACSL) enzymes that mediate Acyl-CoA synthesis (Kim *et al.*, 2001; Van Horn *et al.*, 2005), attenuated the conversion of BODIPY-C12 into BODIPY-TG and reduced the intensity of the intermediate BODIPY-labeled band (Figure 5B, TC, asterisk). Thus BODIPY-C12 needs to be activated by ACSL before incorporation in TG. Of interest, pretreatment of WAT explants with the inhibitor of FFA β-oxidation etomoxir resulted in a higher level of unincorporated BODIPY-C12 and reduction in the

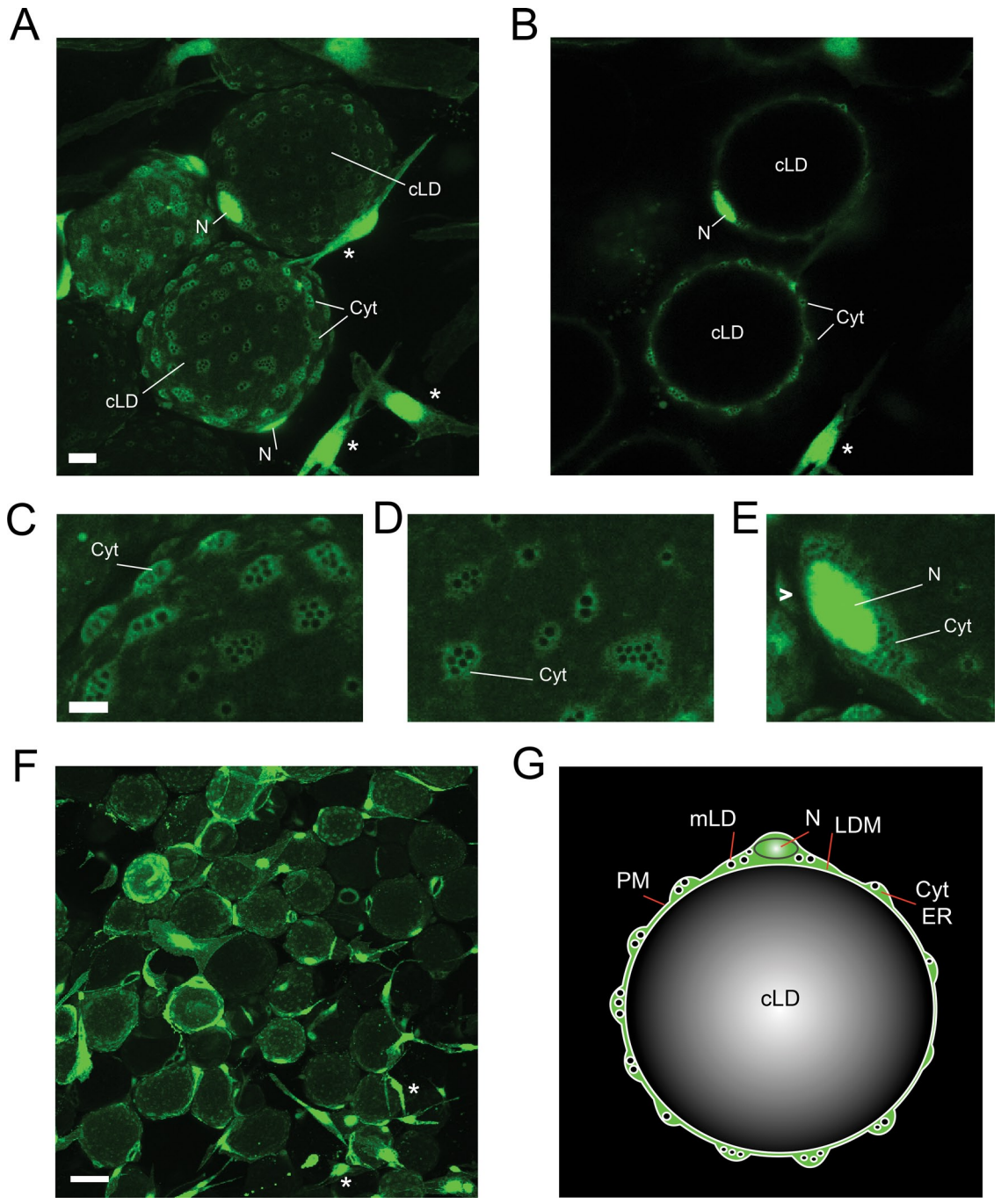

FIGURE 1: Cytoarchitecture of primary unilocular adipocytes. Visceral WAT explants were infected with an adenoviral vector encoding eGFP as described in *Materials and Methods*. On day 2 after infection, live explants were examined for GFP expression using confocal microscopy. cLD, central LD; Cyt, cytoplasm; LDM, lipid droplet membrane; mLD, micro-LD; N, nucleus; PM, plasma membrane. (A) A field of view shows GFP-positive unilocular adipocytes (spheres) and stromovascular cells (asterisks) residing in WAT. The image represents the sum of confocal slices. Bar, 10 μm. (B) Single confocal section of the image in A. Enlarged areas of adipocytes containing cytoplasmic nodules (C, D) and perinuclear cytoplasm (E) filled with GFP-negative spherical cavities. Bar, 5 μm. (F) Portion of the GFP-infected WAT explant shown at lower magnification. Bar, 50 μm. (G) Schematic representation of the spatial organization of a unilocular adipocyte. The cLD of a unilocular adipocyte represents a single sphere tightly fitted inside the cell, whereas the cytoplasm forms multiple nodules containing various organelles.

level of additional BODIPY species (Figure 5B, EX, asterisk), suggesting that BODIPY-C12 can be also metabolized via the β-oxidation pathway. Taken together, this and other studies demonstrate that BODIPY-C12 can be used as a quantitative marker for monitoring basal and insulin-dependent neutral lipid biosynthesis in WAT. Similarly to BODIPY-C12, polyene lipids have been used for measuring FFA metabolism in adipocytes (Kuerschner *et al.*, 2008; Sun *et al.*, 2013).

BODIPY-TG synthesis in WAT explants correlated with the appearance of BODIPY-positive mLDs (Figures 4A and 5A),

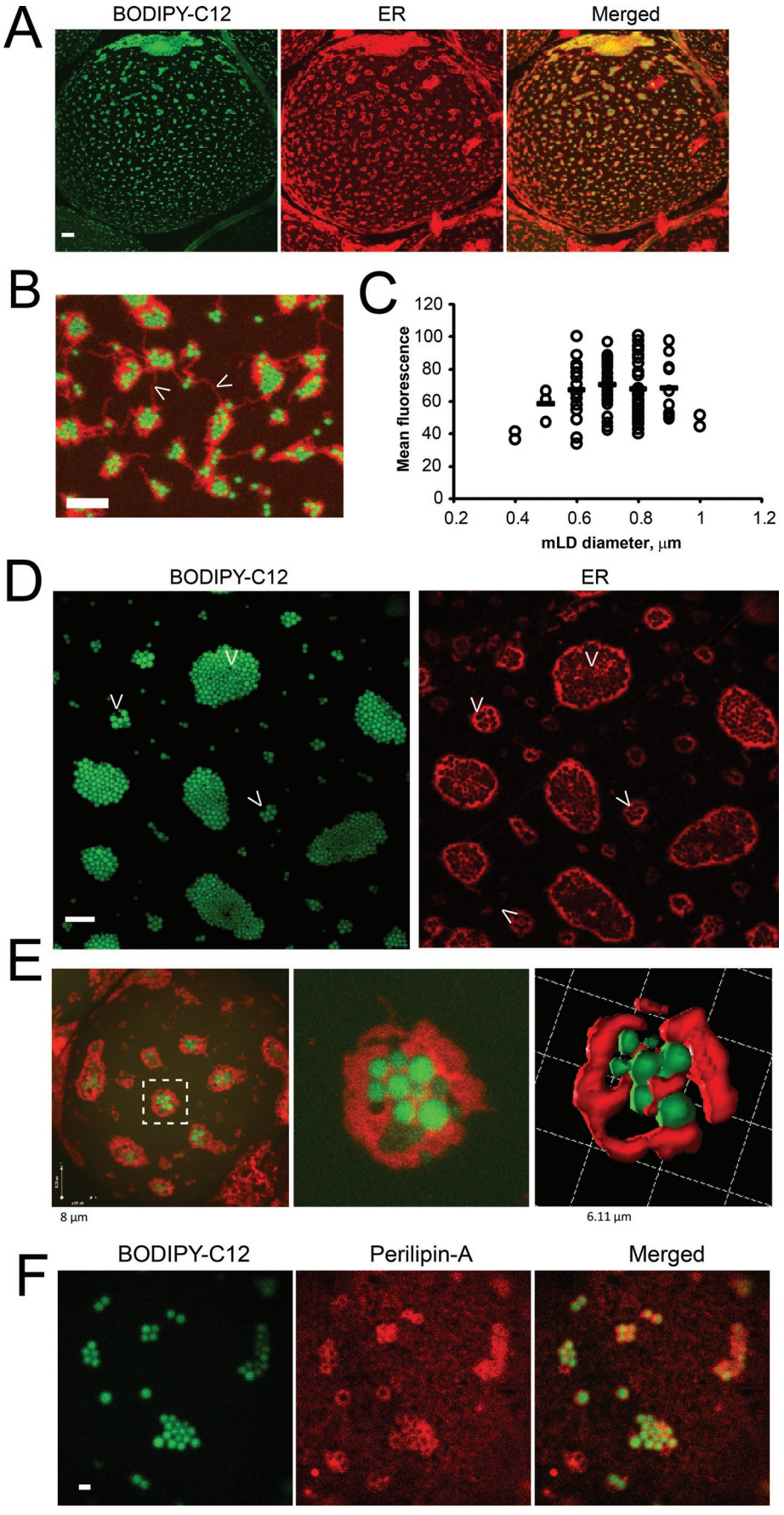

indicating that the transport of BODIPY-C12 into mLDs is coupled to esterification of FFA. To further refine the spatiotemporal kinetics of mLD formation in conjunction with BODIPY-TG biosynthesis, we labeled WAT explants with BODIPY-C12 for shorter periods of time and concurrently followed lipid biosynthesis and intracellular transport by TLC and confocal microscopy, respectively. Under insulin-stimulated conditions, BODIPY-TG was first detected in the cell after a 5-min incubation with BODIPY-C12 (Figure 5C). The kinetics of BODIPY-TG synthesis were similar to that of polyene and radioactive FFA (Kuerschner *et al.*, 2008; Sun *et al.*, 2013). The appearance of TG on TLC corresponded to a significant accumulation of BODIPY fluorescence in mLDs (Figure 5, D, 5 min, and E). Although BODIPY-TG was undetectable on TLC after 1- and 2-min pulse periods (Figure 5C), confocal microscopy revealed dim fluorescent

FIGURE 2: mLDs are associated with the ER in unilocular adipocytes. Visceral WAT explants were incubated for 2 h with 10 nM insulin, labeled with BODIPY-C12 for 15 min, and chased in BODIPY-free medium for 30 min in the presence of the red fluorescent ER-tracker, as described in *Materials and Methods*. (A) Representative confocal image of a BODIPY/ER-labeled adipocyte. Bar, 10 μm. (B) The enlarged area of the adipocyte shows the groups of mLDs (green) surrounded by ER patches (red) attached to the surface of the cLD. Arrowheads indicate ER fibers connecting distinct ER patches. Bar, 5 μm. (C) Size distribution of mLDs ($n = 100$) in the adipocyte (shown in A). Fluorescence intensities of individual mLDs were plotted against their diameters. Horizontal bars are calculated mean intensities of each group of mLDs. The value of 100% on the *y*-axis represents the intensity of the brightest LD in the image. Similar mLD size distributions were obtained in a WAT adipocytes from a large cohort of animals ($n = 38$). (D) Example of the large field of mLDs surrounded by highly fenestrated ER. Bar, 5 μm. (E) Optical reconstruction of the mLD-ER patch; left, whole cell; middle, single patch; right, three-dimensional rendering. (F) Perilipin 1a is associated with mLDs. Insulin-treated WAT explants were labeled for 15 min with BODIPY-C12, chased in label-free medium for 30 min, and fixed in formaldehyde. WAT explants were subjected to indirect immunofluorescence analysis, as described in *Materials and Methods*, using antibodies to perilipin 1a, followed by secondary red fluorescent antibodies. Images represent confocal projections. Bar, 1 μm.

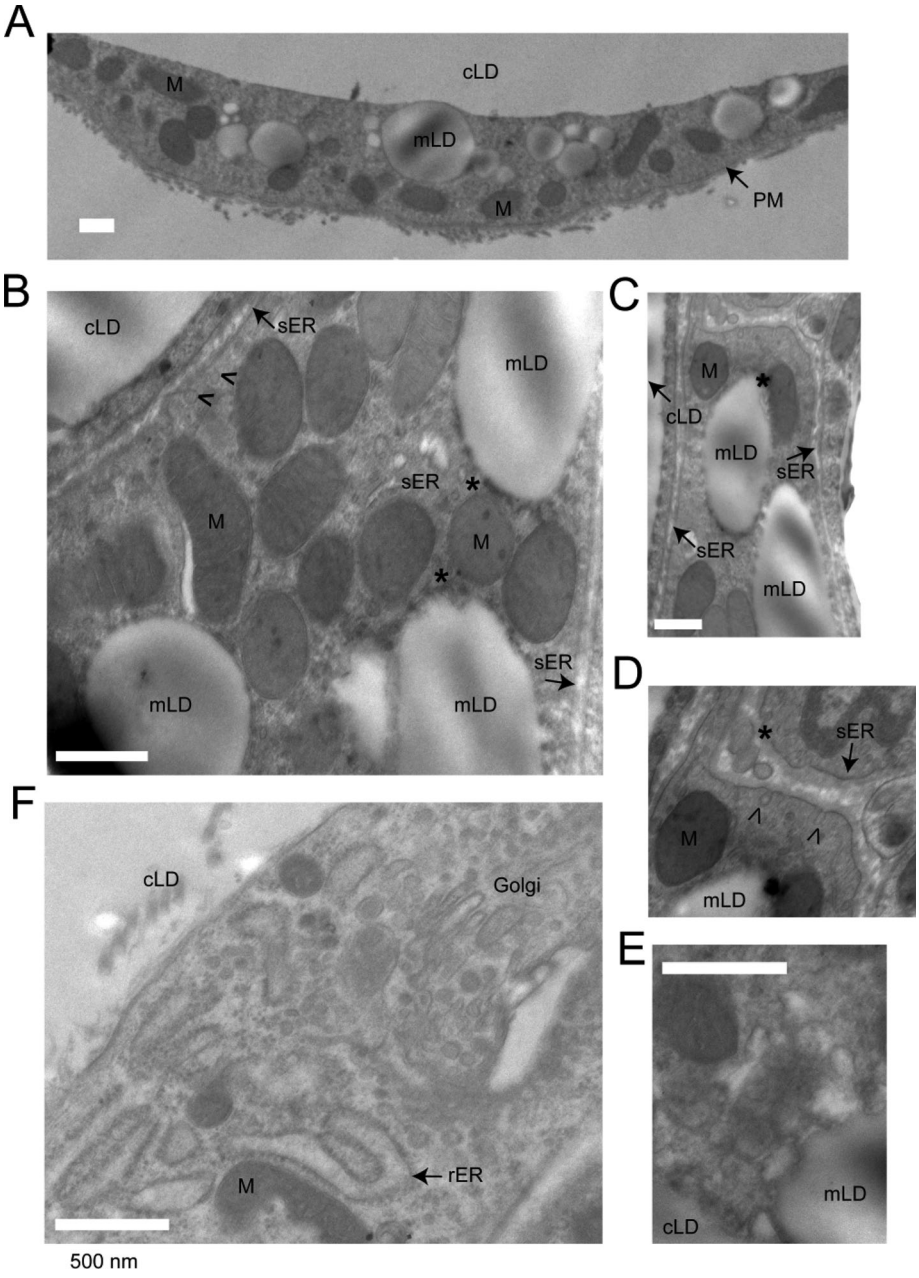

FIGURE 3: Electron microscopy of a unilocular adipocyte. A visceral WAT explant was fixed and processed for electron microscopy, as described in *Materials and Methods*. cLD, central LD; mLD, micro-LD; PM, plasma membrane, rER, rough ER; sER, smooth ER; M, mitochondria. (A) Low-magnification image of the cytoplasmic nodule, containing various organelles. mLDs are in close proximity to the cLD. (B, C) mLDs are associated with mitochondria and the sER. Contact sites between mLDs and mitochondria are marked with asterisks. (B–D) Arrowheads indicate vesicles budding off the ER tubules. (E) Example of a mLD adjacent to electron-lucent vesicular material, which may represent the precursors for mLDs and/or the cross sections of the ER tubules. (F) Area of the adipocyte cytoplasm enriched in the rER (decorated with polyribosomes) and the Golgi. Golgi membranes are surrounded by vesicles containing electron-dense cores. Bar, 500 nM.

speckles associated with the ER (Figure 5E, arrowheads). After 5- and 10-min pulses, most BODIPY fluorescence was associated with "eggs-in-a-nest"-like structures (Figure 5E, asterisks). Pretreatment of WAT explants with triacsin C significantly inhibited the incorporation of BODIPY fluorescence into mLDs and cLDs (Figure 5, F and G). Thus, mLD formation is coupled to TG synthesis in unilocular adipocytes.

DISCUSSION

To better understand the spatiotemporal organization of TG synthesis and packaging in unilocular adipocytes, the most abundant cell type in WAT, we previously developed a unique system for culturing and imaging of WAT explants ex vivo. WAT cultures remain viable and respond to insulin (Varlamov *et al.*, 2010, 2012) and lipolytic stimulation (Varlamov *et al.*, 2013). Previous studies demonstrated that FFA uptake and metabolism in adipocytes can be monitored using fluorescently tagged FFA. For example, polyene FFAs can be metabolized into TG at rates that are similar to those of radiolabeled (Kuerschner *et al.*, 2008) and BODIPY-labeled FFAs (this study; Gong *et al.*, 2011).

The use of fluorescent FFA BODIPY-C12 allowed us to identify novel cell biological features in unilocular adipocytes. The present study demonstrates for the first time that mLDs are intimately associated with the ER patches decorating the surface of the cLD, whereas a significant part of the cLD surface is devoid of ER (Figure 2), indicating that the ER patches are primary sites of TG synthesis in unilocular adipocytes. Furthermore, we observed that the cytoplasm of a unilocular adipocyte is distributed nonuniformly rather than being principally located surrounding the nucleus as previously believed, and forms a series of nodules scattered around the cLD (Figure 1). Because these nodules are also enriched in the ER and mLDs, it is possible that uptake and consequent esterification of FFAs take place inside these structures.

Earlier electron microscopy studies of isolated unilocular adipocytes identified a series of small, 0.5- to 1-μm-diameter LDs associated with the cytoplasmic side of the cLD and surrounded by ER membranes (Cushman, 1970). Our electron microscopy analysis of WAT suggests that mLDs are surrounded by membranes of the smooth ER and mitochondria (Figure 3). Given that etomoxir attenuates FFA utilization in WAT (Figure 5B), it is possible that the "eggs-in-a-nest" structure represents a metabolically active compartment mediating the coupling of insulin signaling to the TG synthesis and the β-oxidation pathways in unilocular adipocytes. The observed inhibition of TG synthesis by etomoxir was surprising. One possible explanation is that acute inhibition of the β-oxidation pathway downregulates glucose transporter-4 expression in adipocytes (Griesel *et al.*, 2010). Because glucose is a substrate for the synthesis of the glycerol backbone of TG, reduced glucose flux may contribute to the observed inhibition of TG formation by etomoxir.

Because mLDs are relatively uniform in size and arranged in a symmetric geometric pattern, it is possible that this unique architecture is achieved by means of protein complexes dynamically

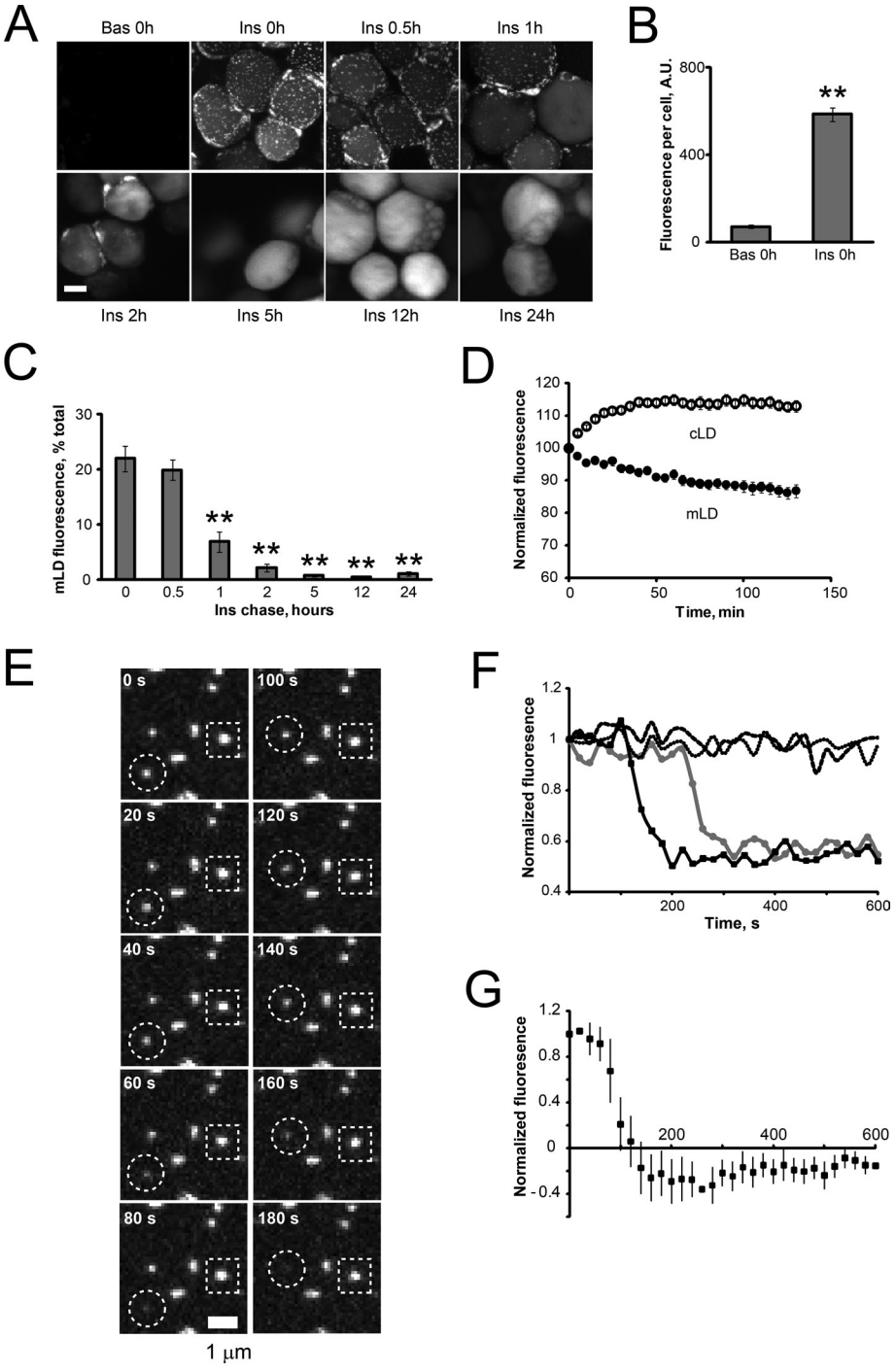

FIGURE 4: Lipid exchange between mLDs and cLDs in unilocular adipocytes. (A–D) Visceral WAT explants were incubated for 2 h under basal conditions or in the presence of 10 nM insulin, labeled with BODIPY-C12 for 15 min, chased in BODIPY-free basal or insulin-containing medium for indicated periods of time, fixed, and examined by confocal microscopy. Bar, 50 μm. (B) Quantification of basal and insulin-stimulated BODIPY-C12 uptake immediately after a 15-min pulse. Error bars represent SEM, $n = 10$. $^{**}p < 0.01$, *t* test. (C) Time course of fluorescence intensities associated with mLDs in insulin-stimulated adipocytes (representative images are shown in A). Error bars represent SEM, $n = 7$–10. $^{**}p < 0.01$, one-way ANOVA followed by *t* test. (D) Time-lapse microscopy of living unilocular adipocytes (Supplemental Video S2). Insulin-stimulated WAT explants were labeled with BODIPY-C12 for 15 min, rinsed in warm medium, and placed on a confocal stage equilibrated to 37°C. Images were recorded in the *xyzt*-mode every 5 min and quantified as described in *Materials and Methods*. Error bars represent SEM, $n = 10$ cells. This experiment was repeated twice with similar results. (E) Dynamics of mLDs. Insulin-stimulated WAT explants were labeled with BODIPY-C12 for 15 min, chased in label-free medium for 30 min, and studied by time-lapse confocal microscopy. Images were recorded in the *xyzt*-mode every 20 s and quantified as described in *Materials and Methods*. Representative snapshot of a BODIPY-C12–labeled adipocyte shows docked mLDs discharging their fluorescent content (circle) or remaining static (square) during a 10-min imaging interval. (F) Two examples of fluorescence traces showing active mLDs (solid lines) and two examples of static mLDs (dashed lines). (G) The average fluorescence trace of active mLDs. Error bars represent SEM, $n = 10$.

associated with the ER/LD interface. For example, the CoA:diacylglycerol acyltransferase (Kuerschner *et al.*, 2008; Yen *et al.*, 2008; McFie *et al.*, 2011)/fatty acid transport protein-1 (Schaffer and Lodish, 1994; Coe *et al.*, 1999; Stahl *et al.*, 2002) complex can facilitate LD expansion, acting at the interface of the LD and the ER (Xu *et al.*, 2012). TG synthesis enzymes can move unidirectionally through bridges connecting the ER and growing LDs (Wilfling *et al.*, 2013). Although the role of the LD-associated ACSL3 (Fujimoto *et al.*, 2004, 2007; Poppelreuther *et al.*, 2012) in LD biogenesis has been investigated (Kassan *et al.*, 2013), further studies are needed to verify the exact mechanism of its action in adipocytes. The present finding that mLDs are outlined by perilipin 1a is consistent with previous reports that perilipin resides in the lipid monolayer of LDs (Blanchette-Mackie *et al.*, 1995; Brasaemle, 2007) and can shuttle between the ER and LD fractions (Skinner *et al.*, 2013). It is likely that the perilipin coat is involved in regulating lipolysis (reviewed in Brasaemle *et al.*, 2009).

The mLDs can transfer their content to the interior of the cLD (Figure 4), suggesting that they may act as intermediate compartments that mediate lipid packaging for long-term storage. We previously demonstrated that LDs can communicate by exchanging fluorescent lipids at LD contact sites in 3T3-L1 adipocytes (Somwar *et al.*, 2011). Li and colleagues have shown that lipid exchange is unidirectional, going from a smaller to a larger LD, and requires the LD contact site–associated protein Fsp27 (CIDEC; Gong *et al.*, 2011). Fsp27 and its interaction with perilipin are required for LD fusion in 3T3-L1 adipocytes (Jambunathan *et al.*, 2011; Grahn *et al.*, 2013; Sun *et al.*, 2013). Because the CIDE-C domain of Fsp27 is necessary and sufficient for the induction of LD growth and the CIDE-N domain of Fsp27 can form a homodimer and increases the efficiency of LD growth (Gong *et al.*, 2011), it has been suggested that the homodimerization of Fsp27 or recruitment of perilipin may promote lipid exchange via a

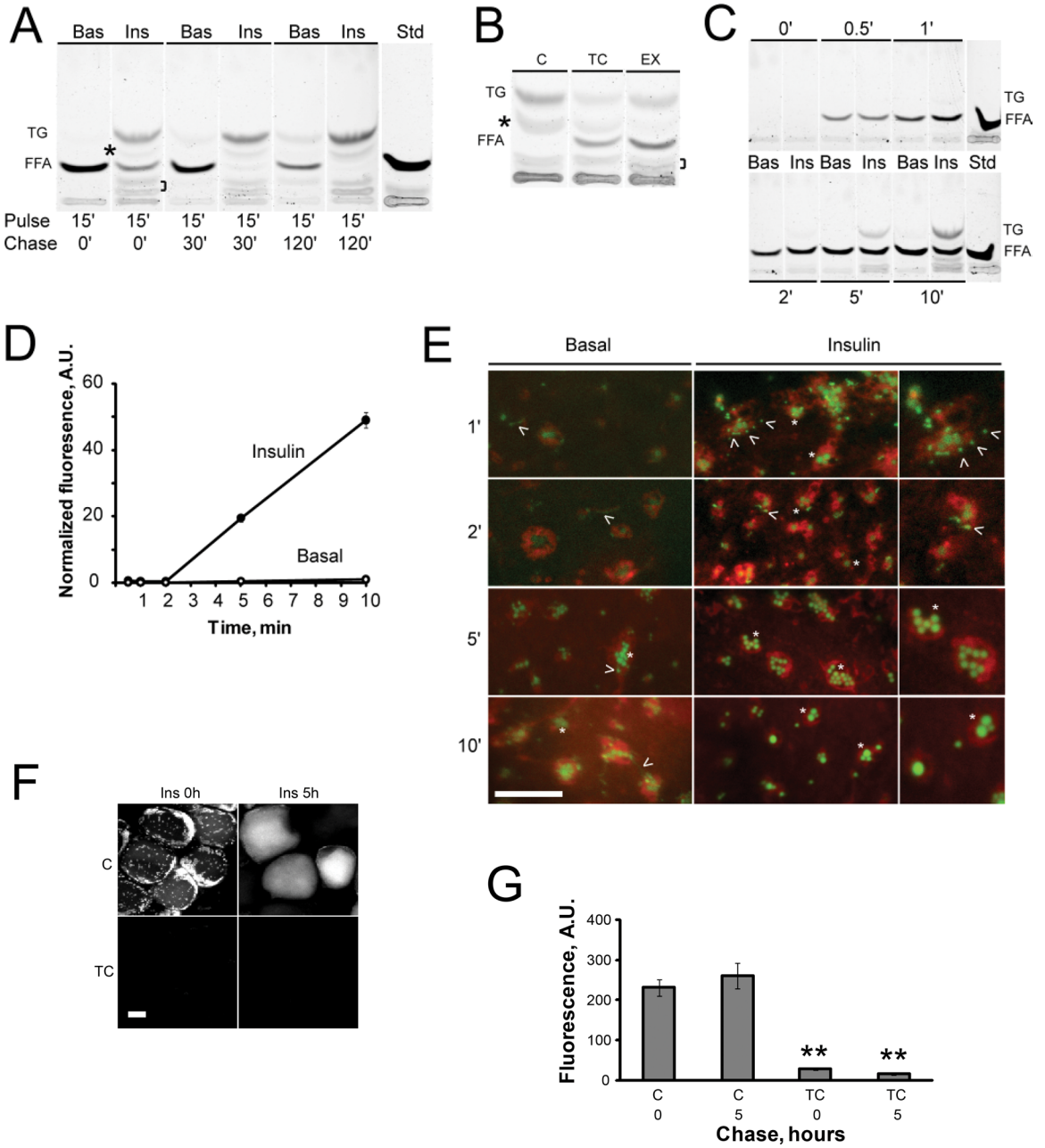

FIGURE 5: Metabolism and intracellular transport of BODIPY-C12 in unilocular adipocytes. (A) Visceral WAT explants were incubated for 2 h in basal medium (Bas) or with 10 nM insulin (Ins), pulsed with BODIPY-C12 for 15 min, and chased in BODIPY-free medium for 0 (lanes 1 and 2), 30 (lanes 3 and 4), or 120 (lanes 5 and 6) min. Lipids were extracted and analyzed by TLC, as described in *Materials and Methods*. The experiment was repeated twice using duplicate WAT explants from the same animal and further verified in WAT from a different animal. Asterisk and bracket indicate the position of BODIPY-labeled products formed in the presence of insulin. (B) WAT explants were incubated for 2 h in control insulin-containing medium alone (C) or in the presence of inhibitors (10 μM triacsin C [TC] or 30 μM etomoxir [EX]), pulsed with BODIPY-C12 for 15 min, and chased in BODIPY-free medium for 120 min with insulin alone or with addition of inhibitors. The experiment was repeated three times with similar results. (C–E) A short time course of BODIPY-C12 metabolism and transport in adipocytes. Two sets of WAT explants were incubated for 2 h in basal medium or with 10 nM insulin, pulsed with BODIPY-C12 for indicated periods of time, and analyzed by TLC (C) or confocal microscopy (D, E). (D) Quantification of mLD-associated fluorescence during a continuous 10-min pulse. Error bars represent SEM, $n = 20$. (E) Representative images showing the progressive accumulation of fluorescence in mLDs (green) in relation to the ER (red) in adipocytes incubated under basal (left) or insulin-stimulated conditions (middle and right). Right, enlargements of the middle. Asterisks, mLDs; arrowheads, BODIPY-positive fluorescent speckles can be seen at earlier incubation times. All images were autoscaled to allow better visualization. Green fluorescence was quantified in D. (F, G) The effect of triacsin C on BODIPY-C12 incorporation in adipocytes. WAT explants were labeled with BODIPY-C12 and chased for 0 or 5 h, as described in Figure 4A, in insulin-containing medium alone or in the presence of10 μM triacsin C. (G) Quantification of intracellular fluorescence. Error bars represent SEM, $n = 10$. $^{**}p < 0.001$, *t* test; A.U., arbitrary units.

putative channel (Sun *et al.*, 2013). The rate of lipid exchange between mLDs and cLD observed in the present study is similar to the rate of LD-LD lipid exchange in 3T3-L1 adipocytes (Gong *et al.*, 2011; Sun *et al.*, 2013), indicating that mLD-cLD communication may involve a similar mechanism. In summary, the present work demonstrates for the first time that TG synthesis in unilocular adipocytes follows a complex spatiotemporal pattern, with mLDs serving as intermediate compartments mediating TG packaging for storage in the large cLD.

MATERIALS AND METHODS

Animals

WAT samples used in this study were obtained as excess tissue from animals studied under protocols previously approved by the Institutional Animal Care and Use Committee of the Oregon National Primate Research Center. Regular chow diet consisted of the two daily meals of Purina LabDiet fiber-balanced monkey chow (15% calories from fat, 27% from protein, and 59% from carbohydrates; no. 5000; Purina Mills, St. Louis, MO), supplemented with fruits and vegetables. Animals used in the present study were lean, insulin-sensitive adult rhesus macaque males and females. Animals were killed according to procedures recommended by the Panel on Euthanasia of the American Veterinary Association. The night before necropsy, food was withheld. Before necropsy, animals were sedated with ketamine in the home cage, transported to the necropsy suite, treated with pentobarbital (25 mg/kg), and exsanguinated by severance of the descending aorta.

TLC

Lipids were extracted and analyzed by TLC as described previously (Sampath *et al.*, 2009). Briefly, 100 mg of WAT was homogenized in chloroform/methanol (2:1, vol/vol), and lipid extracts corresponding to 5 mg of adipose wet weight were dried under a stream of N_2 and resuspended in equal volumes of chloroform/methanol (2:1, vol/vol) for loading onto TLC plates. Plates were developed in heptane/isopropyl ether/acetic acid (60/40/3), and fluorescently labeled lipids were visualized.

BODIPY-C12 uptake in WAT explants

Approximately 5-mm WAT explants were incubated free-floating in plastic 24-well plates filled with 0.4 ml of incubation media. Where indicated, ER-tracker red (BODIPY-Glibenclamide, Life Technologies, Hercules, CA) was added to the media at a 1:1000 dilution. Green fluorescent BODIPY-500/510 C_1, C_{12} (Life Technologies) was prepared in advance by diluting a 2.5 mM methanol stock solution in incubation medium to a final concentration of 10 µM. A 10 µM BODIPY-C12 solution was incubated for 15 min, protected from light, in a 37°C water bath. For fixed-cell analysis, 100 µl of 10 µM BODIPY-C12 solution was added to each well and mixed by repeated pipetting, and the plates were incubated for an additional 15 min at 37°C. Medium was removed by aspiration, tissue was washed three times with warm incubation medium, and incubation was continued for indicated time periods. WAT explants were fixed at room temperature with fresh 4% paraformaldehyde in phosphate-buffered saline (PBS) for 20–30 min, washed four times with PBS, and stored in PBS at 4°C, protected from light, for up to 48 h before confocal analysis.

Indirect immunofluorescence analysis

For immunofluorescence analysis, fixed BODIPY-labeled WAT explants were placed in a 24-well plate containing 500 µl of blocking solution (5% fatty acid–free bovine serum albumin [BSA], 0.4% Triton X-100 in PBS), and incubated gently at room temperature for 1 h. Polyclonal rabbit antibodies to perilipin 1a (Fitzgerald, Acton, MA) were added at a 1:100 dilution and incubated on a rocker overnight at 4°C. WAT explants were washed four times for 5–10 min in blocking solution without BSA, followed by 1-h incubation with secondary antibodies in blocking solution at a 1:1000 dilution. Samples were washed five times with BSA-free blocking solution, followed by two PBS washes, and analyzed by confocal microscopy immediately.

Live-cell imaging

Insulin-treated WAT explants were labeled with BODIPY-C12 for 15 min, transferred into a 35-mm glass-bottom culture dish (MatTek, Ashland, MA) containing 300 µl of medium. Before the experiment, a dish was premounted on a temperature-controlled stage of an inverted Leica SP5 AOBS spectral confocal system (Leica, Wetzlar, Germany) and allowed to equilibrate to 37°C for 30 min. WAT explants were brought to the bottom of the dish with 8 × 8–mm squares of light stainless steel mesh (0.4 mm; TWP, Berkeley, CA) and videorecorded. Confocal microscopy settings were as previously described (Varlamov *et al.*, 2010).

Image processing

Confocal stacks of images were collected at 1-µm intervals and opened with the *LOCI* plug-in data browser, and sum projections were generated using Fiji. mLDs were segmented from the whole cell by manually adjusting the threshold. Three-dimensional rendering was conducted using Volocity 6.2 (Perkin Elmer, Waltham, MA). The diameters and mean intensities of mLDs were determined using the freehand drawing tool. Because some time-lapse movies displayed a minor *x-y* drift, the recursive alignment of stacks of images was performed using the StackReg plug-in. To avoid focal shift (*z*-drift) due to membrane bending or thermal fluctuations, additional series of images were collected below and above the objective focal plane.

Statistical analysis

Statistical differences between groups were determined using the *t* test or one-way analysis of variance (ANOVA), using Prism4 (GraphPad, La Jolla, CA).

Electron microscopy

Dissected WAT explants were fixed in buffered 1.5% glutaraldehyde/1.5% paraformaldehyde. The tissues were then processed in a Ted Pella (Redding, CA) BioWave microwave processor by washing in 0.1 M sodium cacodylate buffer, pH 7.4, postfixed in reduced osmium tetroxide, stained en bloc with 1% uranyl acetate, dehydrated in graded ethanol solutions, and then embedded in epoxy resin. Then 60- to 90-nm-thick sections were placed onto 200-mesh grids, stained with uranyl acetate and lead citrate, and examined with a Tecnai 12 electron microscope at 80 kV (FEI, Hillsboro, OR). Digital images were acquired using a 16-megapixel Advanced Microscopy Techniques (Woburn, MA) camera.

Adenoviral infection of WAT explants

Adenoviral vectors conditionally expressing eGFP were constructed using the approach described by Hardy *et al.* (1997). Briefly, the plasmid pAdtet7-eGFP contains eGFP under the control of a minimal cytomegalovirus promoter fused to the tetracycline operator and a flanking loxP site (Henkel *et al.*, 1998). Adenoviral vectors were generated using homologous recombination in Cre recombinase–expressing CRE8 cells by cotransfection of pAdtet7-eGFP plasmid and E1/E3-deleted conditionally packaged adenovirus genomic DNA (Ad5-ψ5). Recombinant adenoviral vectors were expanded

and virions were concentrated over a sorbitol cushion and tittered on 293A cells. eGFP expression was induced by coinfection with an adenovirus expressing a Tet-off transactivator (Ad-Trans; Streblow *et al.*, 1999). Rhesus WAT explants were exposed to a mix of Adt-eGFP and Ad-Trans at doses ranging from 10^7 to 10^8 plaque-forming units/well. To enhance transduction, adenoviral vectors were preincubated with 100 µg/ml cholesterol for 10 min before addition to cells. Images were collected on day 2 after infection.

ACKNOWLEDGMENTS

We thank Daniel Streblow for provision of adenoviral vectors and reagents and Robert Kayton for help with electron microscopy studies. This work was supported in part by National Institutes of Health grants P50 HD071836 (C.T.R.), K99 DK100640 (H.S.), R21 AG047543 (O.V.), and P51 OD011092 for operation of the Oregon National Primate Research Center.

REFERENCES

Arner P, Bernard S, Salehpour M, Possnert G, Liebl J, Steier P, Buchholz BA, Eriksson M, Arner E, Hauner H, *et al.* (2011). Dynamics of human adipose lipid turnover in health and metabolic disease. Nature 478, 110–113.

Blanchette-Mackie EJ, Dwyer NK, Barber T, Coxey RA, Takeda T, Rondinone CM, Theodorakis JL, Greenberg AS, Londos C (1995). Perilipin is located on the surface layer of intracellular lipid droplets in adipocytes. J Lipid Res 36, 1211–1226.

Bostrom P, Andersson L, Rutberg M, Perman J, Lidberg U, Johansson BR, Fernandez-Rodriguez J, Ericson J, Nilsson T, Boren J, *et al.* (2007). SNARE proteins mediate fusion between cytosolic lipid droplets and are implicated in insulin sensitivity. Nat Cell Biol 9, 1286–1293.

Brasaemle DL (2007). Thematic review series: adipocyte biology. The perilipin family of structural lipid droplet proteins: stabilization of lipid droplets and control of lipolysis. J Lipid Res 48, 2547–2559.

Brasaemle DL, Subramanian V, Garcia A, Marcinkiewicz A, Rothenberg A (2009). Perilipin A and the control of triacylglycerol metabolism. Mol Cell Biochem 326, 15–21.

Brasaemle DL, Wolins NE (2012). Packaging of fat: an evolving model of lipid droplet assembly and expansion. J Biol Chem 287, 2273–2279.

Coe NR, Smith AJ, Frohnert BI, Watkins PA, Bernlohr DA (1999). The fatty acid transport protein (FATP1) is a very long chain acyl-CoA synthetase. J Biol Chem 274, 36300–36304.

Cushman SW (1970). Structure-function relationships in the adipose cell. I. Ultrastructure of the isolated adipose cell. J Cell Biol 46, 326–341.

Fujimoto Y, Itabe H, Kinoshita T, Homma KJ, Onoduka J, Mori M, Yamaguchi S, Makita M, Higashi Y, Yamashita A, *et al.* (2007). Involvement of ACSL in local synthesis of neutral lipids in cytoplasmic lipid droplets in human hepatocyte HuH7. J Lipid Res 48, 1280–1292.

Fujimoto Y, Itabe H, Sakai J, Makita M, Noda J, Mori M, Higashi Y, Kojima S, Takano T (2004). Identification of major proteins in the lipid droplet-enriched fraction isolated from the human hepatocyte cell line HuH7. Biochim Biophys Acta 1644, 47–59.

Gong J, Sun Z, Wu L, Xu W, Schieber N, Xu D, Shui G, Yang H, Parton RG, Li P (2011). Fsp27 promotes lipid droplet growth by lipid exchange and transfer at lipid droplet contact sites. J Cell Biol 195, 953–963.

Grahn TH, Zhang Y, Lee MJ, Sommer AG, Mostoslavsky G, Fried SK, Greenberg AS, Puri V (2013). FSP27 and PLIN1 interaction promotes the formation of large lipid droplets in human adipocytes. Biochem Biophys Res Commun 432, 296–301.

Griesel BA, Weems J, Russell RA, Abel ED, Humphries K, Olson AL (2010). Acute inhibition of fatty acid import inhibits GLUT4 transcription in adipose tissue, but not skeletal or cardiac muscle tissue, partly through liver X receptor (LXR) signaling. Diabetes 59, 800–807.

Hardy S, Kitamura M, Harris-Stansil T, Dai Y, Phipps ML (1997). Construction of adenovirus vectors through Cre-lox recombination. J Virol 71, 1842–1849.

Henkel JR, Apodaca G, Altschuler Y, Hardy S, Weisz OA (1998). Selective perturbation of apical membrane traffic by expression of influenza M2, an acid-activated ion channel, in polarized Madin-Darby canine kidney cells. Mol Biol Cell 9, 2477–2490.

Hommel A, Hesse D, Volker W, Jaschke A, Moser M, Engel T, Bluher M, Zahn C, Chadt A, Ruschke K, *et al.* (2010). The ARF-like GTPase ARFRP1 is essential for lipid droplet growth and is involved in the regulation of lipolysis. Mol Cell Biol 30, 1231–1242.

Jambunathan S, Yin J, Khan W, Tamori Y, Puri V (2011). FSP27 promotes lipid droplet clustering and then fusion to regulate triglyceride accumulation. PLoS One 6, e28614.

Kassan A, Herms A, Fernandez-Vidal A, Bosch M, Schieber NL, Reddy BJ, Fajardo A, Gelabert-Baldrich M, Tebar F, Enrich C, *et al.* (2013). Acyl-CoA synthetase 3 promotes lipid droplet biogenesis in ER microdomains. J Cell Biol 203, 985–1001.

Khor VK, Shen WJ, Kraemer FB (2013). Lipid droplet metabolism. Curr Opin Clin Nutr Metab Care 16, 632–637.

Kim JH, Lewin TM, Coleman RA (2001). Expression and characterization of recombinant rat Acyl-CoA synthetases 1, 4, and 5. Selective inhibition by triacsin C and thiazolidinediones. J Biol Chem 276, 24667–24673.

Kuerschner L, Moessinger C, Thiele C (2008). Imaging of lipid biosynthesis: how a neutral lipid enters lipid droplets. Traffic 9, 338–352.

Li H, Black PN, DiRusso CC (2005). A live-cell high-throughput screening assay for identification of fatty acid uptake inhibitors. Anal Biochem 336, 11–19.

Liao J, Sportsman R, Harris J, Stahl A (2005). Real-time quantification of fatty acid uptake using a novel fluorescence assay. J Lipid Res 46, 597–602.

McFie PJ, Banman SL, Kary S, Stone SJ (2011). Murine diacylglycerol acyltransferase-2 (DGAT2) can catalyze triacylglycerol synthesis and promote lipid droplet formation independent of its localization to the endoplasmic reticulum. J Biol Chem 286, 28235–28246.

Murphy S, Martin S, Parton RG (2010). Quantitative analysis of lipid droplet fusion: inefficient steady state fusion but rapid stimulation by chemical fusogens. PLoS One 5, e15030.

Poppelreuther M, Rudolph B, Du C, Grossmann R, Becker M, Thiele C, Ehehalt R, Fullekrug J (2012). The N-terminal region of acyl-CoA synthetase 3 is essential for both the localization on lipid droplets and the function in fatty acid uptake. J Lipid Res 53, 888–900.

Sampath H, Flowers MT, Liu X, Paton CM, Sullivan R, Chu K, Zhao M, Ntambi JM (2009). Skin-specific deletion of stearoyl-CoA desaturase-1 alters skin lipid composition and protects mice from high fat diet-induced obesity. J Biol Chem 284, 19961–19973.

Schaffer JE, Lodish HF (1994). Expression cloning and characterization of a novel adipocyte long chain fatty acid transport protein. Cell 79, 427–436.

Skinner JR, Harris LA, Shew TM, Abumrad NA, Wolins NE (2013). Perilipin 1 moves between the fat droplet and the endoplasmic reticulum. Adipocyte 2, 80–86.

Somwar R, Roberts CT Jr, Varlamov O (2011). Live-cell imaging demonstrates rapid cargo exchange between lipid droplets in adipocytes. FEBS Lett 585, 1946–1950.

Spalding KL, Arner E, Westermark PO, Bernard S, Buchholz BA, Bergmann O, Blomqvist L, Hoffstedt J, Naslund E, Britton T, *et al.* (2008). Dynamics of fat cell turnover in humans. Nature 453, 783–787.

Stahl A, Evans JG, Pattel S, Hirsch D, Lodish HF (2002). Insulin causes fatty acid transport protein translocation and enhanced fatty acid uptake in adipocytes. Dev Cell 2, 477–488.

Streblow DN, Soderberg-Naucler C, Vieira J, Smith P, Wakabayashi E, Ruchti F, Mattison K, Altschuler Y, Nelson JA (1999). The human cytomegalovirus chemokine receptor US28 mediates vascular smooth muscle cell migration. Cell 99, 511–520.

Sun Z, Gong J, Wu H, Xu W, Wu L, Xu D, Gao J, Wu JW, Yang H, Yang M, *et al.* (2013). Perilipin1 promotes unilocular lipid droplet formation through the activation of Fsp27 in adipocytes. Nat Commun 4, 1594.

Tauchi-Sato K, Ozeki S, Houjou T, Taguchi R, Fujimoto T (2002). The surface of lipid droplets is a phospholipid monolayer with a unique fatty acid composition. J Biol Chem 277, 44507–44512.

Thiam AR, Antonny B, Wang J, Delacotte J, Wilfling F, Walther TC, Beck R, Rothman JE, Pincet F (2013a). COPI buds 60-nm lipid droplets from reconstituted water-phospholipid-triacylglyceride interfaces, suggesting a tension clamp function. Proc Natl Acad Sci USA 110, 13244–13249.

Thiam AR, Farese RV Jr, Walther TC (2013b). The biophysics and cell biology of lipid droplets. Nat Rev Mol Cell Biol 14, 775–786.

Van Horn CG, Caviglia JM, Li LO, Wang S, Granger DA, Coleman RA (2005). Characterization of recombinant long-chain rat acyl-CoA synthetase isoforms 3 and 6: identification of a novel variant of isoform 6. Biochemistry 44, 1635–1642.

Varlamov O, Chu MP, McGee WK, Cameron JL, O'Rourke RW, Meyer KA, Bishop CV, Stouffer RL, Roberts CT Jr (2013). Ovarian cycle-specific regulation of adipose tissue lipid storage by testosterone in female nonhuman primates. Endocrinology 154, 4126–4135.

Varlamov O, Somwar R, Cornea A, Kievit P, Grove KL, Roberts CT Jr (2010). Single-cell analysis of insulin-regulated fatty acid uptake in adipocytes. Am J Physiol Endocrinol Metab 299, E486–496.
Varlamov O, White AE, Carroll JM, Bethea CL, Reddy A, Slayden O, O'Rourke RW, Roberts CT Jr (2012). Androgen effects on adipose tissue architecture and function in nonhuman primates. Endocrinology 153, 3100–3110.
Wilfling F, Thiam AR, Olarte MJ, Wang J, Beck R, Gould TJ, Allgeyer ES, Pincet F, Bewersdorf J, Farese RV Jr, Walther TC (2014). Arf1/COPI machinery acts directly on lipid droplets and enables their connection to the ER for protein targeting. Elife 3, e01607.
Wilfling F, Wang H, Haas JT, Krahmer N, Gould TJ, Uchida A, Cheng JX, Graham M, Christiano R, Frohlich F, Liu X, *et al*. (2013). Triacylglycerol synthesis enzymes mediate lipid droplet growth by relocalizing from the ER to lipid droplets. Dev Cell 24, 384–399.
Wu Q, Kazantzis M, Doege H, Ortegon AM, Tsang B, Falcon A, Stahl A (2006a). Fatty acid transport protein 1 is required for nonshivering thermogenesis in brown adipose tissue. Diabetes 55, 3229–3237.
Wu Q, Ortegon AM, Tsang B, Doege H, Feingold KR, Stahl A (2006b). FATP1 is an insulin-sensitive fatty acid transporter involved in diet-induced obesity. Mol Cell Biol 26, 3455–3467.
Xu N, Zhang SO, Cole RA, McKinney SA, Guo F, Haas JT, Bobba S, Farese RV Jr, Mak HY (2012). The FATP1-DGAT2 complex facilitates lipid droplet expansion at the ER-lipid droplet interface. J Cell Biol 198, 895–911.
Yen CL, Stone SJ, Koliwad S, Harris C, Farese RV Jr (2008). Thematic review series: glycerolipids. DGAT enzymes and triacylglycerol biosynthesis. J Lipid Res 49, 2283–2301.